

## Fast Wave Antenna Loading in Advanced Tokamak Plasmas in DIII-D

R.I. Pinsky,<sup>1</sup> F.W. Baity,<sup>2</sup> R.H. Goulding,<sup>2</sup> C.M. Greenfield,<sup>1</sup> J.C. Hosea,<sup>3</sup>  
M. Murakami,<sup>2</sup> C.C. Petty<sup>1</sup>, and G. Wang<sup>4</sup>

<sup>1</sup>General Atomics, P.O. Box 85608, San Diego, California 92186-5608, USA

<sup>2</sup>Oak Ridge National Laboratory, Oak Ridge, Tennessee USA

<sup>3</sup>Princeton Plasma Physics Laboratory, Princeton, New Jersey USA

<sup>4</sup>University of California, Los Angeles, California USA

The goal of the present work is to measure the fast wave current drive (FWCD) antenna loading in regimes of Advanced Tokamak (AT) interest to estimate the maximum power that will be coupled reliably to those discharges with the present antennas. DIII-D is equipped with three FWCD systems, one of which is capable of generating up to 2.0 MW at 60 MHz and the other two being capable of operation in a range of frequencies from 60-120 MHz (presently limited to 1.0 MW from each transmitter at 120 MHz). Each transmitter drives a four-element phased array antenna, with the antennas being referred to by their toroidal angle in the DIII-D vacuum vessel: 285 is driven by the 60 MHz transmitter, and 0 and 180 each driven by one of the 60-120 MHz transmitters. The reason for the interest in the highest available frequency (120 MHz) for FWCD applications is that the efficiency of electron current drive at that frequency has been shown [1] to be substantially higher than is obtained at 83 MHz and 60 MHz, owing primarily to decreased parasitic absorption on the fast ion population at high cyclotron harmonics.

Previous work has shown that the FWCD systems drive current consistent with theory in ELMing H-mode plasmas [2,3] even under conditions of fairly low single-pass absorption, provided that the edge density profile is such that the fast wave cutoff layer is just outside the separatrix, which in turn is not too close to the vessel wall. In these ELMing H-modes, this condition is obtained when the ELM frequency is lower than about 100 Hz. Unfortunately, the same edge condition that increases the current drive efficiency tends to reduce the time-averaged resistive loading on the antennas (and hence increase the antenna voltage for a given power level.) In turn, this means that the regimes of interest for current drive tend to have low antenna power limits.

### I. Antenna Loading Measurements in AT-Relevant Plasmas

A principal application of the FWCD systems is in AT discharges, both to provide a source of electron heating without fueling in the center of the discharge and to provide an actuator for control of the central noninductive current density. Measurements of the FWCD antenna loading in such discharges were undertaken in 2003. The plasmas were in a pumped double-null configuration, with 6-10 MW of NBI, 3.5 MW of electron cyclotron heating (five gyrotrons) and were at a toroidal field of 1.85 T and a plasma current of 1.2 MA. The plasmas were in a vigorously ELMing (ELM frequency of about 70 Hz) H-mode throughout the period of the measurement. The 0 deg and 285 deg FW antennas,

at 117.6 MHz and 60 MHz respectively, were used at power levels of less than 0.4 MW on each system. The 285 antenna was used in either co-current (i.e., phased at 90 deg in a direction to increase the plasma current) or counter-current drive phasing, while the 0 deg antenna was used only in co-current phasing in this experiment.

The distance between the separatrix and the outer wall limiting surface, known as the “outer gap”, was varied either dynamically during the rf pulse or from shot-to-shot. The surface of the antenna Faraday screens (single-layer and  $\sim 50\%$  optically opaque on both antennas, tilted on the 0 deg antenna at an angle of 12 deg, horizontal on the 285 antenna) is recessed by about 3 cm behind the bumper limiters. The series-resonant load resistance (per current strap) of both arrays as a function of the outer gap is shown in Fig. 1, from discharges with dynamic gap variation over a 1 second period. The plotted points correspond to the loading between ELMs. Since the antenna loading in the absence of plasma is almost entirely due to resistive losses in the antenna and transmission lines, the vacuum loading has been subtracted from the data shown here. (Due to the higher frequency used and longer transmission lines, the vacuum loading of the 0 deg array is more than twice that of the 285 array —  $0.23 \Omega$  and  $0.11 \Omega$  respectively.) The  $e$ -folding decay length for the antenna loading has been predicted with a very simple one-dimensional planar model, in which the fast waves are assumed to be as evanescent as they are in vacuum all the way up to the right-hand cutoff and the poloidal spectrum of the finite-height antennas is ignored. The predicted decay length agrees quite well with the observed behavior of the 0 deg antenna loading, while the 285 antenna loading appears to decline more rapidly than the model predicts as the gap increases. The absolute value of the loading (not predicted by the simple model) is higher for the 0 deg antenna at 117.6 MHz than for the 285 antenna at 60 MHz, so the maximum voltage in the antenna and feedline is smaller for a given applied power on the 0 deg antenna. The larger resistive loading presented to the feedline by the 0 deg antenna is most likely due to the two-segment strap design [5] being nearly self-resonant at 117.6 MHz (not a result of different wave physics). The loading on the 285 antenna is observed to be larger in co-current phasing than in counter-current phasing, which is observed on DIII-D whenever co- and counter-phasing are compared in identical discharges. The phenomenon is explained as a consequence of the static magnetic field line tilt and the poloidal spectrum launched by the antenna in Ref. [6].

A significant improvement over the previous work on FWCD in ELMing H-mode plasmas on DIII-D is that the edge density profiles were measured at high time resolution with an FM

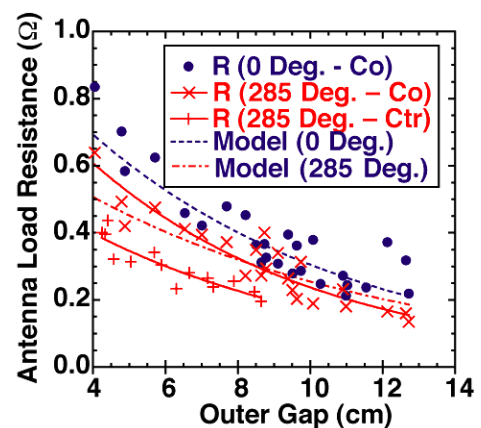


Fig. 1. Series-resonant load resistance for both arrays as a function of outer gap, measured between ELMs.

microwave reflectometer system [7]. A sequence of edge density profiles measured between ELMs from the dynamic gap ramp shows that the edge density profile is indeed rigidly translated along with the separatrix in such a ramp. The same diagnostic was used to measure the edge density profiles just prior to, during, and immediately after single ELMs, at outer gaps of 4.6 cm and 8.3 cm (Fig. 2). The cutoff density for the fast waves is about  $3\text{--}4 \times 10^{18} \text{ m}^{-3}$  [3] and the face of the antennas is at a major radius of about  $R = 2.39 \text{ m}$ . Hence, the measured density profiles show that the radial distance from the cutoff layer to the antenna face at the peak of the ELM density pulse is small and similar in the two cases shown. Therefore the antenna loading at the peak is expected to be large and roughly independent of the outer gap. This qualitative expectation is borne out by the loading data from a large number of ELMs; for example, the peak in loading during ELMs for the 285 antenna in co-phasing is about  $1 \Omega$  throughout the outer gap ramp, while the loading between ELMs, shown in Fig. 1, ranges from  $0.2$  to  $0.6 \Omega$ .

An important practical result from the experiment was that an outer gap of  $<6 \text{ cm}$  for more than a second led to excessive heating of first-wall components owing to fast ion losses during high-power NBI. However, the confinement and stability of the plasma were not adversely affected by outer gaps down to  $6 \text{ cm}$ , so that future experiments should be conducted with as small an outer gap as the heating of the first wall allows. As NB power is replaced with rf power (FWCD and ECH) that does not create fast ion populations, presumably smaller outer gaps than  $6 \text{ cm}$  will be useable.

## II. Voltage and Power Limits and ELMs

Were it not for the complicating effect of ELMs, prediction of the maximum reliable coupled power in a given discharge would be straightforward, armed with measurements of the antenna loading and previous measurements of the reliable peak voltage handling of the antenna in the presence of plasma. In the present case, the  $0 \text{ deg}$  antenna loading at  $117.6 \text{ MHz}$  in the case of a  $6 \text{ cm}$  outer gap, between ELMs, is  $0.8 \Omega$  (including the vacuum loading). Operation into ELMing H-mode plasmas at  $83 \text{ MHz}$  with this antenna in 1997-1998 was possible at peak voltages around  $25 \text{ kV}$  (vacuum conditioning levels exceeded  $30 \text{ kV}$ ), and reliable around  $20 \text{ kV}$ . At  $0.8 \Omega$  loading, peak voltages of  $25 \text{ kV}$  ( $20 \text{ kV}$ ) would yield a net power level of  $1.6 \text{ MW}$  ( $1.0 \text{ MW}$ ). With a vacuum loading due to resistive losses of  $0.23 \Omega$ , the coupled power fraction at this gap is  $71\%$ , so that the coupled power would be  $1.14 \text{ MW}$  ( $0.73 \text{ MW}$ ). The voltage drops drastically at each ELM due to the increase in

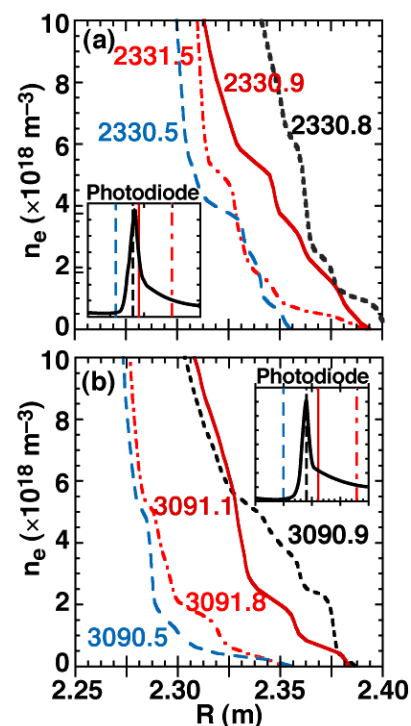


Fig. 2. Edge density profiles during an ELM, at outer gaps of (a)  $4.6 \text{ cm}$  and (b)  $8.3 \text{ cm}$ .

loading, so that in this simple picture the time-averaged coupled power would be somewhat larger than these numbers indicate by an amount proportional to the ELM duty factor. These numbers motivate an upgrade to the final stage amplifier in the 0 deg system to raise the power capability at 115-118 MHz from 1.0 MW to the 1.5-2.0 MW range.

However, the effect of ELMs on the antenna voltage standoff capability is very substantial, as has been recently studied in detail on ASDEX Upgrade [8,9]. Although the antenna voltage drops during an ELM owing to the increase in loading, it is found on both ASDEX and on DIII-D that an ELM has a significant probability of triggering an antenna breakdown. As was observed on DIII-D in 1993 and described in Ref. [2], an ELM can ignite a “balanced fault”, which was interpreted as an rf-sustained glow discharge within the antenna boxes. An example of arcs being associated with ELMs is shown in Fig. 3, where the 0 deg antenna experiences 14 ELMs in an 0.2 s period, with three ELMs causing trips at peak voltages less than 12 kV.

For the FW systems to reach their full potential for applications to the AT program, the most urgent need is to develop conditioning techniques and/or modifications to the antennas that lead to reliable standoff voltages higher than 30 kV in the presence of vigorously ELMing H-mode plasmas, or replacement of the antennas with much lower impedance structures, such as the poloidally segmented antenna discussed in Ref. [10]. In fact, a double poloidal strap design such as is used in ASDEX Upgrade and in the 0 and 180 deg antennas on DIII-D is already a first step in the direction of a poloidally segmented antenna. Along the lines of modification of existing antennas, Ref. [9] suggests reconsideration of an optically opaque Faraday screen to reduce the plasma density in the antenna boxes due to ELMs.

This work was supported by the U.S. Department of Energy under DE-FC02-04ER54698, DE-AC05-00OR22725, DE-AC02-76CH03073, and DE-FG03-01ER54615.

- [1] C.C. Petty, *et al.*, Plasma Phys. Control. Fusion **43**, 1747 (2001).
- [2] R.I. Pinsker, *et al.*, Proc. of 25th Euro. Conf. on Controlled Fusion and Plasma Phys., Prague, 1998, Vol. **22C** (European Physical Society) p. 1406.
- [3] C.C. Petty, *et al.*, Nucl. Fusion **39**, 1421 (1999).
- [5] F.W. Baity, *et al.*, in Radio Frequency Power in Plasmas (Proc. 10<sup>th</sup> Top. Conf., Boston, 1993) (New York: AIP,1994) p. 343.
- [6] E.F. Jaeger, *et al.*, Nucl. Fusion **38**, 1 (1998).
- [7] L. Zeng, *et al.*, Plasma Phys. Control. Fusion **46**, A121 (2004).
- [8] V. Bobkov, *et al.*, J. Nucl. Materials **313-316**, 956 (2003)
- [9] V. Bobkov, *Studies of High Voltage Breakdown Phenomena on ICRF Antennas*, IPP Garching Rpt. IPP 4/282 (2003)
- [10] G. Bosia and S. Bremond, in Radio Frequency Power in Plasmas (Proc. 15<sup>th</sup> Top. Conf., Moran, WY, 2003) (New York: AIP,2003) p. 82.

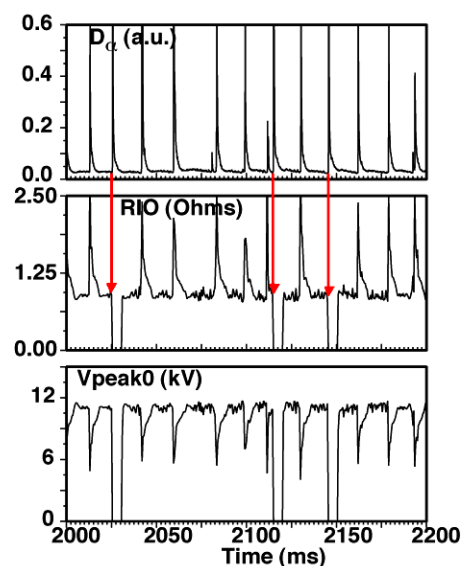


Fig. 3. Arcs triggered by ELMs on the 0 deg array.